STAR FORMATION AND YOUNG POPULATION OF THE H II COMPLEX Sh2-294

M. R. SAMAL[1,2], A. K. PANDEY[1], D. K. OJHA[3], N. CHAUHAN[1], J. JOSE[1], AND B. PANDEY[4]

[1] Aryabhatta Research Institute of Observational Sciences, Nainital 263129, India; manash.samal@oamp.fr
[2] Laboratoire d'Astrophysique de Marseille (UMR 7326 CNRS & Université d'Aix-Marseille), 38 rue F. Joliot-Curie, 13388 Marseille Cedex 13, France
[3] Tata Institute of Fundamental Research, Mumbai 400005, India
[4] Physics Department, D.S.B. Campus, Kumaun University, Nainital 263129, India

ABSTRACT

The Sh2-294 H II region ionized by a single B0V star features several infrared excess sources, a photodissociation region, and also a group of reddened stars at its border. The star formation scenario in this region seems to be quite complex. In this paper, we present follow-up results of Sh2-294 H II region at 3.6, 4.5, 5.8, and 8.0 μm observed with the *Spitzer Space Telescope* Infrared Array Camera (IRAC), coupled with H_2 (2.12 μm) observation, to characterize the young population of the region and to understand its star formation history. We identified 36 young stellar object (YSO, Class I, Class II, and Class I/II) candidates using IRAC color–color diagrams. It is found that Class I sources are preferentially located at the outskirts of the H II region and associated with enhanced H_2 emission; none of them are located near the central cluster. Combining the optical to mid-infrared (MIR) photometry of the YSO candidates and using the spectral energy distribution fitting models, we constrained stellar parameters and the evolutionary status of 33 YSO candidates. Most of them are interpreted by the model as low-mass ($<4\,M_\odot$) YSOs; however, we also detected a massive YSO ($\sim 9\,M_\odot$) of Class I nature, embedded in a cloud of visual extinction of $\sim$24 mag. Present analysis suggests that the Class I sources are indeed a younger population of the region relative to Class II sources (age $\sim 4.5 \times 10^6$ yr). We suggest that the majority of the Class I sources, including the massive YSOs, are second-generation stars of the region whose formation is possibly induced by the expansion of the H II region powered by a $\sim 4 \times 10^6$ yr B0 main-sequence star.

Key words: H II regions – ISM: individual objects (Sh2-294) – stars: formation – stars: pre-main sequence

Online-only material: color figures, machine-readable table

1. INTRODUCTION

The massive OB stars have a profound influence on the evolution of molecular clouds and consequently influence star formation. The stellar radiation and winds due to massive stars in the region can sweep low-density interstellar matter, consequently forming a dense layer of gas at the periphery of H II regions, or they can compress existing primordial clumps. In both processes, the matter at the later stage becomes unstable against self-gravity to form young protostars. These are commonly known processes that can induce a new generation of star formation around expanding H II regions (see, e.g., Sugitani et al. 2002; Deharveng et al. 2005; Chauhan et al. 2009; Samal et al. 2010; Ojha et al. 2011). Sh2-294 ($\alpha_{2000} = 07^h16^m34\overset{s}{.}5$, $\delta_{2000} = -09°26'38''$) is an H II region powered by a B0V star and is possibly interacting with a molecular cloud, thus creating a photon-dominated region (PDR) that can be seen toward the eastern side as polycyclic aromatic hydrocarbon (PAH) emission in the *Midcourse Space Experiment* (*MSX*) *A* band (Samal et al. 2007; Paper I). Using multiwavelength observations, Samal et al. (2007) have studied the stellar content and the distribution of ionized and dust emission in the region. They identified two groups of stars, one of which is associated with the B0V star at the center of the optically visible nebula. The second group (termed as "region A") is situated at the eastern side of the optical cluster and near the peak of 8 μm emission along the PDR. Samal et al. (2007), using the optical color–magnitude diagram and theoretical evolutionary models, estimated the age of the ionizing source as 4×10^6 yr, whereas low-mass pre-main-sequence (PMS) stars show an age spread of $(1–5) \times 10^6$ yr. On the basis of the youth of the sources in region A (age $\leqslant 1 \times 10^6$ yr) compared to the age of the ionizing

source ($\sim 4 \times 10^6$ yr), Samal et al. (2007) suggested Sh2-294 as a site of triggered star formation. However, the mechanism that is responsible for the initiation of new star formation in this region is still not clearly understood and requires proper identification and characterization of stellar sources present in the region to get a step ahead. On the basis of high-resolution near-infrared (NIR) and optical observations, Yun et al. (2008) estimated the age of the ionizing source of Sh2-294 as 4×10^6 yr but suggested a higher age for the PMS sources. Due to the absence of spectroscopic or longer wavelength ($\lambda > 2.2\,\mu$m) observations, the exact nature and evolutionary status of the PMS sources in the region has not been studied so far. Now with the high angular resolution of *Spitzer Space Telescope*, it is possible to make a more reliable membership census of the young stellar objects (YSOs) with the disk and envelope of the region, as 3–8 μm bands of *Spitzer* reduce the degeneracy between selective interstellar extinction and intrinsic IR excess. Moreover, the nature of YSOs can be best discovered using their broadband spectral energy distributions (SEDs) and their comparison with more sophisticated radiative transfer SED-fitting models (e.g., Robitaille et al. 2007). Thus, in conjunction with the available photometric data sets for the region, the *Spitzer* observations will allow us to characterize the individual YSOs with their SEDs and constrain their evolutionary status, thus helping to establish the spatial and temporal relationship among the YSOs. Therefore, we revisited the region at near- and mid-infrared windows for the follow-up study of the Sh2-294 star-forming region (SFR), to have a better picture of star formation activity. The distance to Sh2-294 is uncertain and varies from 3.2 kpc to 4.8 kpc (Moffat et al. 1979; Samal et al. 2007; Yun et al. 2008). In this work, we adopted an average distance of 4.0 kpc for our analysis and organized

the paper with the following layout. We describe the *Spitzer* observations and data reduction techniques in Section 2. In Section 3, the observational results are presented, which include the morphology of the region, the identification of the YSOs, and their properties obtained with the SED modeling. The star formation scenario in the region is discussed in Section 4, and Section 5 summarizes our results.

2. OBSERVATIONS AND DATA REDUCTION

The archived MIR data for the region were obtained with the Infrared Array Camera (IRAC; Fazio et al. 2004b) on board the *Spitzer Space Telescope*. IRAC has four wavelength bands centered at 3.6, 4.5, 5.8, and 8.0 μm, each of which has a field of view of $\sim$5′.2 $\times$ 5′.2. The pixel size in all four bands is $\sim$1″.22. The corrected basic calibrated data (BCD) images were downloaded from the *Spitzer Space Telescope* Archive using the Leopard package. The IRAC observations of the region were taken on 2006 November 25 (Program ID 30734, AOR key 18902784: Massive Star Clusters, PI: Donald Figer). Mosaics were built at the native instrument resolution of 1″.22 pixel^{-1} with the standard BCDs using the Mosaicker and Point Source Extractor software program provided by Spitzer Science Center.

We performed aperture photometry on the IRAC images using the DAOPHOT package of IRAF, with a source detection at the 5σ level above the average local background. Due to the crowded nature of the field, an aperture radius of 2 pixels and a sky annulus extending from 2 to 6 pixels were used. We adopted the zero-point magnitudes for the standard aperture radius (10 pixels) and background annulus (10–20 pixels) of 19.67, 18.92, 16.86, and 17.39 mag in the 3.6, 4.5, 5.8, and 8.0 μm bands, respectively, and the appropriate aperture corrections were made using the values described in the IRAC Data Handbook.[5] To estimate the contamination due to non-YSO candidates, we analyzed a control field (Program ID 30734, AOR key 18902784: Galactic structure, PI: Steven Majewski) located approximately 1°.1 away from the target field with no obvious signs of star formation, using the same procedure as described above. For both fields the sources that have photometric uncertainties less than 0.2 mag are considered good detections. This should be considered as a conservative lower limit as the calibration uncertainty associated with the IRAC bands is 2%–3% and, in addition, there is 1%–2% uncertainty in the aperture corrections.

3. RESULTS

3.1. Morphology of Sh2-294

Figure 1 shows a color composite image of Hα emission (taken from Paper I) superimposed with the IRAC 8 μm emission. The plus symbol in the image marks the position of the exciting source of Sh2-294. The position of the massive B1.5 source associated with "region A" is marked with an asterisk symbol (see Section 1). The 8 μm IRAC band contains emission bands at 7.7 and 8.6 μm commonly attributed to PAH molecules. PAHs are believed to be destroyed in the ionized gas but thought to be excited in the PDR at the interface of the H II region and molecular cloud by the absorption of far-UV photons leaking from the H II region. Therefore, PAHs are good tracers of the hot PDR that surrounds the H II region.

Figure 1 also reveals the distribution of 8 μm emission in a filamentary fashion, with its long axis aligned in the east–west

---

[5] http://irsa.ipac.caltech.edu/data/SPITZER/docs/irac
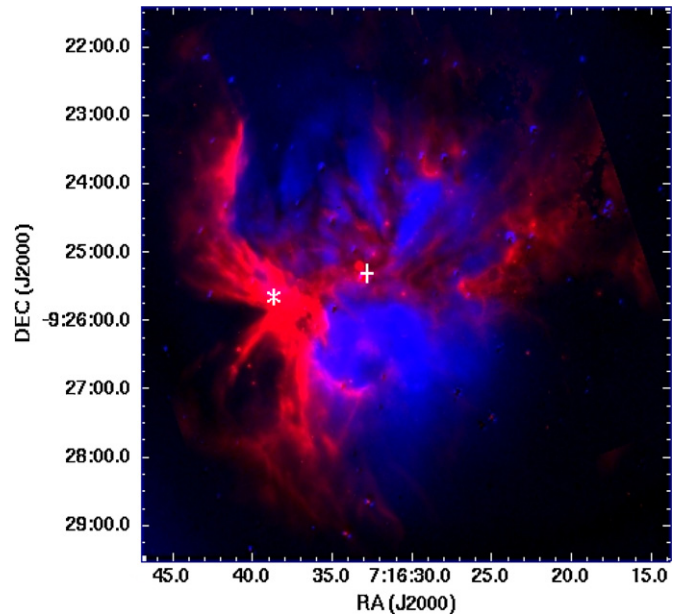
Figure 1. *Spitzer*-IRAC 8 μm image (red) superimposed on Hα line image (blue) of the Sh2-294 region. The image has a field of view of $\sim$8′ $\times$ 8′. The plus and asterisk symbols show the positions of the exciting source of Sh2-294 and of the massive B1.5 source at its border, respectively.

(A color version of this figure is available in the online journal.)

direction that bisects the H II region and the ionized gas appearing to be streaming away orthogonal to the long axis. On both sides of the filament axis, the ionized gas shows a decrease in intensity possibly due to the density gradient in the original medium. The ionized gas is bounded more in the eastern direction as compared to in the western direction; however, the overall morphology of the nebula looks bipolar in nature. The bipolar morphology has been noticed in NIR to MIR bands in few H II regions and/or bubbles (see, e.g., Churchwell et al. 2006; Saito et al. 2009). Now long-wavelength observation ($>$100 μm) with *Herschel* has added new insight to this morphology. For example, the recent finding by Deharveng et al. (2012) with *Herschel* observations, the H II region "Sh2-201," illustrates a clear bipolar morphological nature, with two bipolar lobes perpendicular to a dense neutral filament extending east–west. The two lobes seem to be bounded by cold neutral material of low column density ($\leqslant 10^{21}$ cm^{-2}), whereas the column density is high ($>10^{22}$ cm^{-2}) on each side at the waist of Sh2-201 along the parental filament (Deharveng et al. 2012). Bipolar H II regions are believed to be formed in a filamentary cloud. Due to the absence of sensitive long-wavelength observations, it is hard to imagine the shape and structure of the original cloud, on the large scale in which Sh2-294 has formed. However, we shall discuss the importance of H II region evolution in a filamentary cloud as well as in a hierarchical clumpy cloud from the perspective of future star formation processes in Section 5.1.

3.2. Identification of Young Stellar Objects

The circumstellar dust emission from the disk and infalling envelope of YSOs gradually disappears with time. The sequence of evolutionary phases of a YSO are generally described as: embedded in a circumstellar envelope and an accretion disk (Class I); a Classical T Tauri star surrounded by an optically thick disk (Class II); and a weak-line T Tauri star with an optically thin disk (Class III) and are generally classified
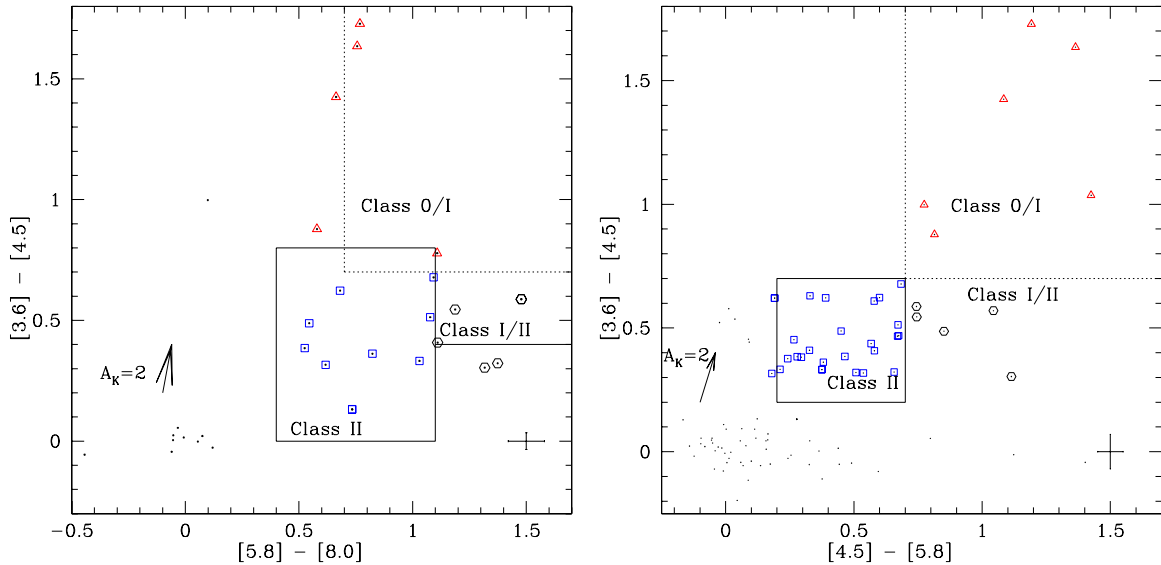
Figure 2. Left: IRAC [3.6]–[4.5]/[5.8]–[8.0] CC diagram with boxes representing the boundaries of different classes of sources. Right: IRAC [3.6]–[4.5]/[4.5]–[5.8] CC diagram with boxes representing the boundaries of different classes of sources (see the text for details). A reddening vector of $A_K = 2$ mag, using the extinction law of Flaherty et al. (2007), and mean error bars of the colors are shown in both IRAC CC diagrams.

(A color version of this figure is available in the online journal.)

Table 1
Photometric Data at IRAC Bands

| R.A. (deg) J2000	Decl. (deg) J2000	[3.6] (mag)	[4.5] (mag)	[5.8] (mag)	[8.0] (mag)
109.124010	−9.495950	11.942 ± 0.009	11.927 ± 0.012	11.942 ± 0.023	11.949 ± 0.076
109.167320	−9.489430	11.075 ± 0.006	11.054 ± 0.009	11.135 ± 0.015	11.060 ± 0.045
109.142310	−9.485300	9.981 ± 0.004	10.008 ± 0.005	9.995 ± 0.009	9.875 ± 0.040

(This table is available in its entirety in a machine-readable form in the online journal. A portion is shown here for guidance regarding its form and content.)

with slopes of SEDs between 2 and 20 μm (Lada & Wilking 1984; Lada 1987). The IRAC [3.6]–[4.5]/[5.8]–[8.0] and [3.6]–[4.5]/[4.5]–[5.8] color–color (CC) diagrams are also used as tools to identify different classes of sources (e.g., Allen et al. 2004; Hartmann et al. 2005) and follow a similar classification. Restricting our analysis to the sources having photometric error less than 0.2 mag, we detected 102 sources in the 3.6, 4.5, and 5.8 μm bands and 31 sources in all the IRAC bands in a common area of ∼6′.8 × 6′.8. These catalogs are made after removing three sources that appear to be extended and/or multiple sources in the high-resolution H$_2$ (2.12 μm) and 3.6 μm IRAC images. The final catalog used to identify the YSOs in the present analysis is given in Table 1. A sample of Table 1 is given here, whereas the complete table is available in electronic form as part of the online material. The H$_2$ mosaic image was constructed using the observations made with the ISAAC camera of the Very Large Telescope (VLT). The data were retrieved from the ESO archive.[6] Further details about the observations are described in Yun et al. (2008).

The IRAC [3.6]–[4.5]/[5.8]–[8.0] CC diagram is shown in the left panel of Figure 2. Following the classification scheme by Allen et al. (2004) and Hartmann et al. (2005), the regions in the CC diagram occupied by Class II, Class I/II, and Class 0/I objects are indicated. The sources with the color of the stellar photosphere are centered around (0, 0); they include foreground, main-sequence (MS), and Class III objects. The objects with

$0.0 \leqslant$ [3.6]–[4.5] $\leqslant 0.8$ and $0.4 \leqslant$ [5.8]–[8.0] $\leqslant 1.1$ are classified as Class II objects. The boundary for Class II sources is marked with a box and is represented by squares. The dotted lines with [3.6]–[4.5] $\geqslant 0.7$ and [5.8]–[8.0] $\geqslant 0.7$ distinguish Class 0/I (triangles) sources from Class II sources (Hartmann et al. 2005). The zone with [5.8]–[8.0] $\geqslant 1.1$ and [3.6]–[4.5] between 0.0 and 0.7 can be occupied by Class 0/I/II sources. Since Class 0 sources are generally not visible at wavelengths shorter than 10 μm, these objects are likely to be Class I/II sources and are shown with hexagon symbols. On the basis of the above criteria, the [3.6]–[4.5]/[5.8]–[8.0] CC diagram yields 20 YSOs. The search of YSOs on the basis of the IRAC [3.6]–[4.5]/[5.8]–[8.0] CC diagram might have been affected by the lower sensitivity of the IRAC 8.0 μm band to detect faint sources and also by the bright background PAH emission. Therefore, in order to detect additional YSOs, we use the IRAC [3.6]–[4.5]/[4.5]–[5.8] CC diagram shown in the right panel of Figure 2. Hartmann et al. (2005) show that the division between Class II and Class III T Tauri stars occurs at [3.6]–[4.5] ∼ 0.2 and [4.5]–[5.8] ∼ 0.2, with Class III stars generally situated at [3.6]–[4.5] < 0.2 and [4.5]–[5.8] < 0.2, whereas most of the Class I/0 protostars are located at [3.6]–[4.5] $\geqslant 0.7$ and [4.5]–[5.8] $\geqslant 0.7$. The region with [4.5]–[5.8] $\geqslant 0.7$ and [3.6]–[4.5] between 0.2 and 0.7 is less defined, and the overlap between Class I and Class II sources can be seen in well-studied SFRs (e.g., Muench et al. 2007; Koenig et al. 2008). On the basis of the above studies, we classify the sources that fall within or in the close vicinity of the boundaries marked in the [3.6]–[4.5]/[4.5]–[5.8] CC diagram. They are

---

[6] http://archive.eso.org/eso/eso-archive-main.html

3
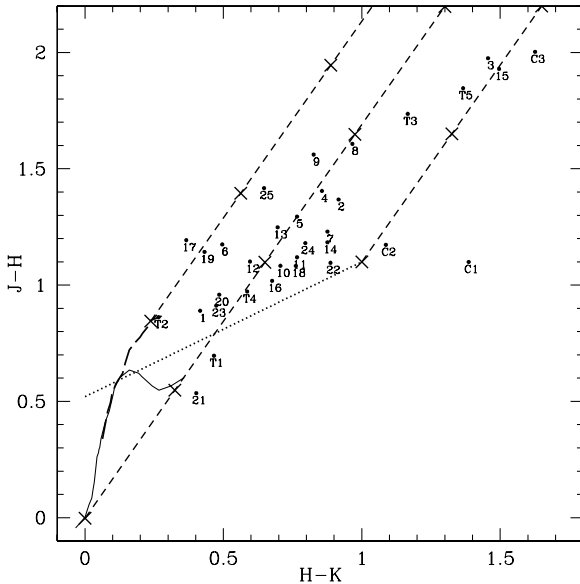
Figure 3. NIR CC diagram for all the YSOs that have JHK counterparts. The thin solid line and thick dashed curves represent the unreddened MS and giant branches (Bessell & Brett 1988), respectively. The dotted line indicates the locus of intrinsic CTTSs (Meyer et al. 1997). The curves and the colors are converted to the California Institute of Technology system. The parallel dashed lines are the reddening vectors drawn from the tip of the giant branch ("upper reddening line"), from the base of the MS branch ("middle reddening line"), and from the base of the tip of the intrinsic CTTS line ("lower reddening line"), with crosses at every 5 mag of visual extinction. The numbers 1–25 represent IRAC Class II sources, whereas T1–T5 and C1–C3 denote the Class I/II and Class I sources, respectively. The magnitudes for C1 and C2 in J and H bands are the upper limit; therefore, their locations in the CC diagram are not real.

marked as Class II (squares), Class I (triangles), and Class I/II (hexagon) in Figure 2. It is to be noted that all the sources that show characteristics of YSOs in the IRAC [3.6]–[4.5]/[5.8]–[8.0] CC diagram are also identified as YSOs in the [3.6]–[4.5]/[4.5]–[5.8] CC diagram. However, it is possible that some of the sources identified as Class II may be reddened field stars/Class III sources.

The sample of YSOs identified on the basis of the MIR CC diagram may be contaminated by background dusty active galactic nuclei and asymptotic giant branch stars as they have colors similar to those of YSOs. In nearby SFRs, Fazio et al. (2004a) found that 50% of the sources with [3.6] mag > 14.5 are extragalactic in nature. In our sample, we have only three common sources in the first three bands of IRAC that have [3.6] mag > 14.5. We visually inspected these sources in VLT H_2 and *Spitzer* 3.6 μm images, and in both images they appear as a point-like stellar object. We used a statistical approach to estimate the contamination in the sample of the identified YSOs by comparing the MIR CC diagram of a control field (not shown) located at $\alpha_{2000} = 07^h14^m49^s$, $\delta_{2000} = -10°27'39''$ having an almost equal area to that of the Sh2-294 H II region. Using the same diagnostic approach as described above, we find only three objects lying in the Class II and Class I zone of the MIR CC plot. This comparison suggests that the expected number contamination to the YSO population of the Sh2-294 region is likely to be less than 10%.

Figure 3 shows the $J - H/H - K$ CC diagram for the identified YSOs. The NIR counterparts were identified using a matching radius of 1″.22. In Figure 3, the IRAC-classified Class II, Class I/II, and Class I YSOs are labeled with the numbers 1–25, T1–T5, and C1–C3, respectively. The majority of the

identified YSOs (barring T1 and 21) lie above the locus of the Classical T Tauri stars (CTTSs) given by Meyer et al. (1997), indicating that these could be the probable CTTSs. A comparison of the positions of these YSOs in the NIR CC diagram (see Figure 3) with the CC diagram of the control field (see Figure 9(b) of Samal et al. 2007) again suggests that most of the sources identified using IRAC CC diagrams are most likely YSO candidates. However, the positions of sources 17, 19, 21, and T2 in the NIR CC diagram are not compatible with those of Class II sources. Sources 17, 19, and T1 fall in the close vicinity of the leftmost reddening vector that starts from the tip of the unreddened giant locus, whereas the position of source 21 falls far below the T Tauri locus. The positions of these sources in the NIR CC diagram also mimic the positions of the field star distribution of the control field. Moreover, the spatial positions of three sources (17, 19, and 21) show that they are away from the cluster center (see Section 3.4).

From IRAC photometry, we find a total of 36 likely YSO candidates, indicating that star formation is still active in the region. It is not possible to distinguish Class III YSOs from the MS and/or field stars with the existing photometric data alone. Spectroscopic data and/or X-ray observations are needed to confirm the YSO nature of the Class III sources. The X-ray emission in the case of Class III stars is elevated by a factor of 10^3–10^4 compared to the MS stars (Walter & Barry 1991). In the present analysis, we restrict ourselves to this more reliable sample of Class I and Class II YSOs. In the following sections, we have used the spatial distribution of the identified YSOs and their characteristics to study the star formation scenario in the Sh2-294 H II complex.

3.3. H_2 Structures

The morphology of the Sh2-294 region (see Figure 1) suggests that as the ionized gas streams away from the center, it possibly encounters an inhomogeneous medium, illustrating patchy, clumpy, and knotty structures, which can be seen in *Spitzer* 8 μm emission. In order to correlate the structures seen in 8 μm, the positions of the detected YSOs, and the H_2 emissions, we used the deep image at the 2.12 μm, 1–0 $S(1)$ line of H_2, obtained with the VLT. The present H_2 image is considerably more sensitive and has higher angular resolution than that presented in Paper I. Figure 4 displays the H_2 image at 2.12 μm, which reveals strong emission along the eastern border of the H II region, as well as notable features at various locations of the nebula, which are numbered #1 to #5. The diffuse H_2 emission can be excited by Lyman and Werner UV photons (e.g., Chrysostomou et al. 1992) from the massive stars and thus can trace the PDR or can be due to collisional excitation in the presence of shocks arising from outflows from nearby YSOs. For dense gas ($n_H \sim 10^5$ cm^{-3}), H_2 emission alone cannot be used to identify the PDR as UV excitation levels can be collisionally redistributed (see Allen et al. 1999); hence, another PDR tracer like PAH emission is necessary to trace the PDR around a nebula (Giard et al. 1994). Though the spectroscopic observations of H_2 lines and their ratios would rather provide the exact nature of the excitation (see Luhman et al. 1998), close resemblance of diffuse H_2 emission with the 8 μm emission (see Figure 1) suggests that the H_2 emissions at the periphery of Sh2-294 are more likely caused by UV fluorescence. The identified H_2 structures are of particular interest as they show rim- or arc-like morphology, with either the rim facing toward the ionizing source at the center or the curvature of the arc (e.g., #2) appearing to be created by the UV photons of an ionizing star. The morphology suggests that
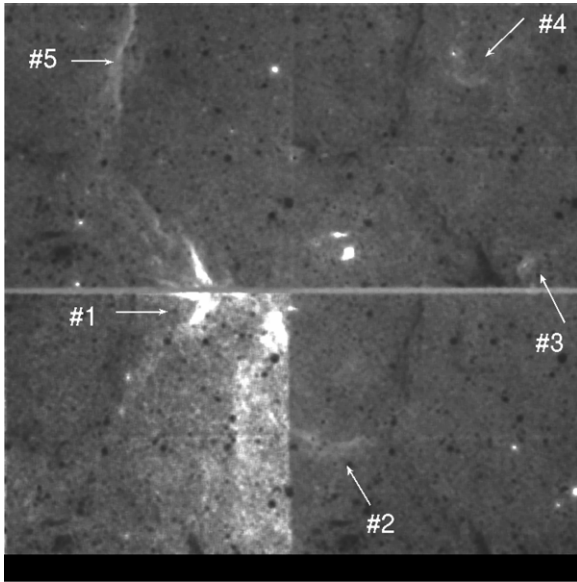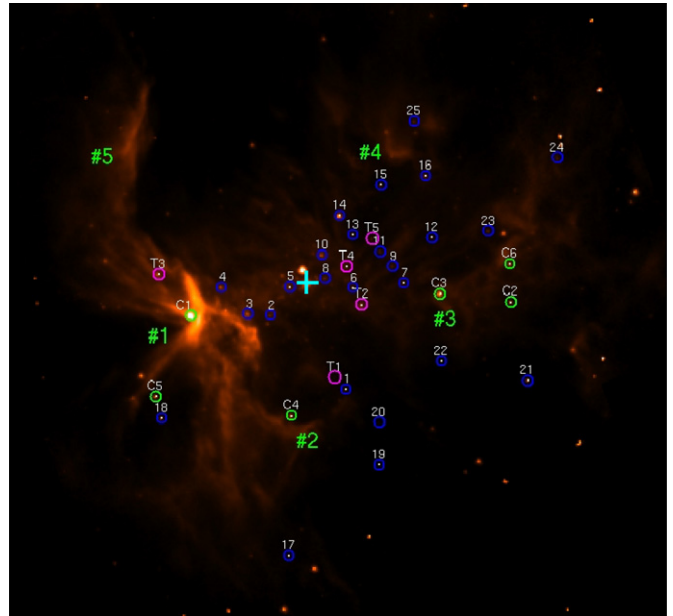
Figure 4. H$_2$ image at 2.12 μm, median smoothed with the stars subtracted. The positions of the enhanced emissions are marked as numbers. The point-like sources seen in the above smoothed image are the product of the residuals that left in the case of bright saturated stars. The image is centered on $\alpha_{2000} = 17^{h}16^{m}32^{s}$, $\delta_{2000} = -09°25'32''$ and has a field of view of $\sim 5'.2 \times 5'.2$. North is up and east is to the left.

Figure 5. Spatial distributions of Class II (blue circles), Class I (green circles), and Class I/II (magenta circles) overlaid on the 5.8 μm image. The image has a field of view of $\sim 7'.2 \times 7'.2$ and is centered on $\alpha_{2000} = 17^{h}16^{m}32^{s}$, $\delta_{2000} = -09°25'32''$. The YSOs are labeled in the same manner as in Figure 3. The plus symbol shows the position of the ionizing source. The enhanced H$_2$ structures are leveled as in Figure 4. North is up and east is to the left.

(A color version of this figure is available in the online journal.)

the weak H$_2$ and PAH emissions associated with the Sh2-294 region possibly correspond to UV excited positions of the dense condensations or fragments of the original molecular cloud in which Sh2-294 was born. However, high-resolution and highly sensitive molecular line observations are needed to reveal the truth. Here, we presume that these dusty structures are associated with the Sh2-294 SFR because the rims/carved arcs are facing toward the ionizing star and exhibit externally heated structures, as expected in the case of a motionless cloud exposed to strong UV radiation from nearby massive star(s).

3.4. Spatial Distribution of YSOs

We identified 36 YSOs (6 Class I, 25 Class II, and 5 Class I/II) using IRAC CC diagrams; the spatial distribution of these YSOs on the 5.8 μm image is shown in Figure 5. The YSOs are labeled in the same manner as in Figure 3. Figure 5 indicates that the YSO candidates are preferentially located in/around regions with diffuse 5.8 μm emission. It is found that all the Class I sources are located at the outer regions, whereas the majority of the Class II sources are found to be concentrated around the proximity of the ionizing source. If Class I sources are really the precursors to Class II sources, as expected from their less evolved circumstellar environments, they should have younger ages. Hence, the distribution of Class I sources indicates that the star formation seems to be continued near the outer parts of the H II region. The YSOs C1, C2, C3, C4, C6, 1, and 25 are of particular interest because of their association with the H$_2$ structures (as marked in Figure 5) and PAH emissions.

The IRAC sensitivity and bright diffuse PAH emissions at 5.8 and 8.0 μm band could be one of the issues for the detection of a lower number of YSOs. We carried out the quantitative evaluation of the completeness of the photometric data with respect to the brightness and the position by adding artificial stars to both 5.8 and 8.0 μm images. The ratio of the number of stars recovered to those added in each magnitude interval gives the completeness factor as a function of magnitude. We

found that the completeness in the central region is $\sim 80\%$ to the level of ~ 14.0 mag and ~ 12.0 mag at 5.8 μm and 8.0 μm, respectively. However, in the regions of diffuse emissions (e.g., #1), the completeness decreases to 50% at magnitudes ~ 14.0 and ~ 12.0 at 5.8 μm and 8.0 μm, respectively. Only one Class I YSO has been identified in region #1 on the basis of IRAC data. The lower detection of YSOs could be the result of a decrease in sensitivity due to the bright PAHs, as is obvious from the completeness analysis.

3.5. Physical Properties of YSOs

To get deep insight into the nature of the YSOs identified in the present work, we constructed SEDs using the models and fitting tools of Robitaille et al. (2006, 2007). The models are computed using a Monte-Carlo-based radiation transfer code (Whitney et al. 2003a, 2003b), which uses several combinations of the central star, accreting disk, infalling envelope, and bipolar cavity for a reasonably large parameter space. Interpreting SEDs using the radiative transfer code is subject to degeneracies, and spatially resolved multiwavelength observations can break the degeneracy. To constrain the parameters of the stellar photosphere and circumstellar environment, we fit the SEDs to only those sources for which we have a minimum of six data points in the wavelength range from 0.55 to 8 μm. We search the counterparts of the identified YSOs in the optical–NIR bands by Yun et al. (2008) and in the Two Micron All Sky Survey (2MASS) Point Source Catalog (Cutri et al. 2003), using a matching radius of 1''.22. This yields 33 sources detected in six bands or more ranging from optical (VRI) to IRAC (3.6, 4.5, 5.8, 8.0 μm) bands, which include 21 sources having optical counterparts. Out of 33 sources that have a minimum of six data points, 25 of them have fluxes at four wavebands of the Wide-field Infrared Survey Explorer (WISE; Wright et al. 2010) survey. The WISE bands have central wavelengths at 3.4, 4.6,
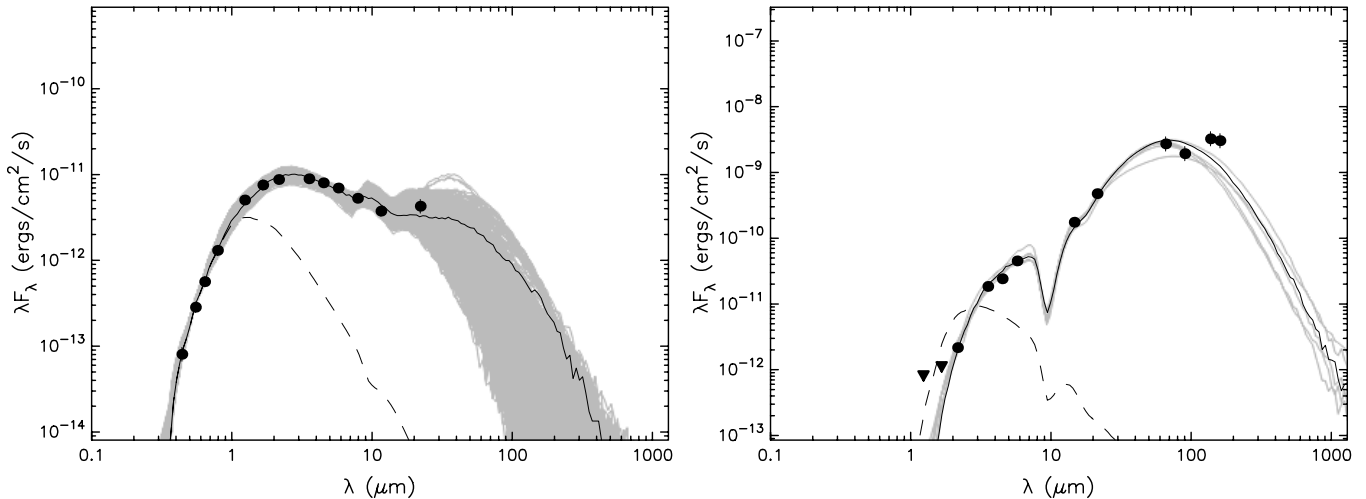
Figure 6. SEDs for a Class II (left) and a Class I (right) source. Left: the SEDs for source 14. The black line shows the best fit, and the gray lines show subsequent good fits with $\chi^2 - \chi^2_{\min} \leqslant 2N_{\mathrm{data}}$. The dashed line shows the stellar photosphere corresponding to the central source of the best-fitting model. The filled circles denote the input flux values. Right: the SED for source C1. The lines have the same meaning as in the left panel. The filled circles denote the input flux values. The triangles are upper limits for the flux values at J and H bands, taken from 2MASS. The flux values at 14.65 and 21.30 μm are from the *MSX* Point Source Catalog (Egan et al. 2003) for source G224.1880+01.2407, and the fluxes at 65, 90, 140, and 160 μm are from the AKARI Far-Infrared Surveyor catalog (Yamamura et al. 2009) for source 0716378-092559.

12, and 22 μm, with spatial resolutions of 6″.1, 6″.2, 6″.5, and 12″.0, respectively. As stated in Robitaille (2008), the SED-fitting tool deals with a single source, and input fluxes from multiple sources in a beam can result in incorrect stellar age and mass. Similarly, any erroneous fluxes can seriously affect the chances of obtaining a sensible SED and thus sensible physical parameters. As there is strong clustering of point sources seen in the IRAC 4.5 μm image (not shown), along with bright nebulosities found in the WISE 12 μm and 22 μm image, we therefore limited the use of WISE fluxes by preferring IRAC 3.6 μm and 4.5 μm fluxes over the WISE 3.4 μm and 4.6 μm, due to superior spatial resolution of IRAC bands. Similarly, we use only those fluxes at 12 μm and 22 μm as inputs that have good-quality flags. We also set an upper limit at 22 μm for those sources for which we do not have detection, by assigning the minimum 22 μm flux that is found in our sample of YSOs. The SED-fitting tool fits each of the models to the data, allowing the distance and external foreground extinction to be free parameters. Since we do not have spectral-type information for our identified YSOs, in order to derive their approximate extinction values, we traced back these sources along the reddening vector to the intrinsic late MS locus or its extension in the NIR CC diagram (e.g., Tej et al. 2006). Considering the uncertainties that might have gone into the estimates, we used the estimated value $A_V \pm 2.5$ mag as an input parameter for these sources. For Class I sources, for which we do not have NIR data, we allow A_V up to 30 mag. We further set 10%–30% error in the flux estimates due to possible uncertainties in the calibration and intrinsic object variability. Figure 6 shows an example of SEDs of the resulting models for the Class II and Class I sources. We obtained physical parameters for all the sources adopting an approach similar to that of Robitaille et al. (2007) by considering those models that satisfy $\chi^2 - \chi^2_{\min} \leqslant 2N_{\mathrm{data}}$, where $\chi^2_{\min}$ is the goodness-of-fit parameter for the best-fit model and N_{data} is the number of input observational data points. The parameters are obtained from the weighted mean and the standard deviation of these models, weighted by $e^{(-\chi^2/2)}$ of each model, and are shown in Table 2. These parameters are obtained from the set of models that represent the overall distribution and therefore

more likely suppress any extreme values that may arise due to a few badly fitted models. However, due to limited observational data points, some of the parameters from the model fits can be narrowly constrained over others depending on the available fluxes. Since we are mainly interested in stellar parameters due to the availability of shorter wavelength fluxes, we therefore only quote a few parameters from the 14 parameter space SED models. Table 2 lists the stellar mass ($M_\star$), stellar temperature ($T_\star$), stellar age ($t_\star$), mass of the disk (M_{disk}), disk accretion rate ($\dot{M}_{\mathrm{disk}}$), foreground visual absorption (A_V), and $\chi^2_{\min}$ of the best fit. Table 2 reveals that the ages of the majority of Class II YSO candidates (excluding 17) vary between 1.5 and 7×10^6 yr with a median age of $(4.5 \pm 1.9) \times 10^6$ yr, whereas the visual extinction varies from 3.2 to 13.5 mag, indicating the presence of non-uniform extinction within the region. Out of 25 Class II sources, 18 have fluxes at optical wavelengths; thus, their age estimations are expected to be better constrained, with a median age of $(5.1 \pm 1.4) \times 10^6$ yr. From Table 2, it appears that the YSOs identified in the present work are detected nearly down to $\sim$1.8 $M_\odot$ and probably a large number of low-mass YSOs are embedded in the cloud. We note that the stellar ages given in Table 2 are only approximate. Spectroscopic observations of the YSOs would be more accurate in the determination of their stellar age. In the Robitaille et al. (2007) models, the stellar masses and ages are sampled using the isochrones and evolutionary tracks (Bernasconi & Maeder 1996; Siess et al. 2000) from the stellar luminosity and temperature, derived from the SED models. Since the age determination for all the YSOs is being made following the same set of evolutionary tracks and the same approach, we therefore use the relative age among the YSOs to constrain the star formation history of the complex. However, we are aware of the fact that the age estimation depends on the choice of isochrones. For example, Hillenbrand et al. (2008) suggested that the use of a different set of isochrones can lead to a systematic uncertainty at a level of 0.75 dex for sub-solar mass stars, though the agreement is better for older PMS solar mass stars. Out of six Class I sources identified in the present study, only three (C1, C2, and C3) have sufficient data points to fit the models of Robitaille et al. (2007). The models

Table 2
Inferred Physical Parameters from SED Fits to YSOs

ID	R.A. (deg) (J2000)	Decl. (deg) (J2000)	M_* ($M_\odot$)	T_* (10^3 K)	t_* (10^6 yr)	M_{disk} ($M_\odot$)	$\dot{M}_{disk}$ (10^{-8} $M_\odot$ yr^{-1})	A_V (mag)	χ^2
1	109.130424	−9.443050	1.99 ± 0.36	5.83 ± 1.23	4.85 ± 2.64	0.009 ± 0.012	3.97 ± 3.66	3.82 ± 0.59	2.82
2	109.145180	−9.428912	2.19 ± 0.37	8.68 ± 1.64	6.99 ± 2.42	0.006 ± 0.013	3.44 ± 3.42	8.13 ± 0.53	0.89
3	109.149498	−9.428577	3.00 ± 0.47	11.03 ± 1.80	5.10 ± 2.41	0.003 ± 0.009	1.12 ± 1.61	13.59 ± 1.15	8.05
4	109.154785	−9.423507	2.53 ± 0.53	8.01 ± 2.13	4.45 ± 1.33	0.004 ± 0.007	4.47 ± 4.54	8.72 ± 0.50	0.98
5	109.141357	−9.423445	2.87 ± 0.65	9.75 ± 3.12	4.99 ± 2.43	0.005 ± 0.016	2.30 ± 2.77	7.61 ± 0.73	1.05
6	109.128922	−9.423709	2.24 ± 0.35	9.01 ± 1.57	7.66 ± 1.62	0.001 ± 0.003	0.84 ± 0.86	7.35 ± 0.67	4.07
7	109.118996	−9.422717	2.25 ± 0.34	9.14 ± 1.52	7.55 ± 1.34	0.001 ± 0.004	0.75 ± 0.81	7.56 ± 0.52	20.35
8	109.134392	−9.421776	2.44 ± 0.55	7.65 ± 2.72	4.47 ± 2.79	0.007 ± 0.016	3.36 ± 4.55	10.90 ± 0.90	2.28
9	109.121185	−9.419425	3.50 ± 0.83	7.49 ± 4.17	1.56 ± 0.98	0.011 ± 0.018	10.83 ± 10.68	10.03 ± 1.50	4.85
10	109.135048	−9.417233	4.85 ± 0.31	16.10 ± 1.03	4.93 ± 0.98	0.000 ± 0.001	0.04 ± 0.04	6.64 ± 0.30	7.30
11	109.123581	−9.416539	2.31 ± 0.48	5.69 ± 1.03	3.23 ± 2.24	0.010 ± 0.019	2.80 ± 2.65	6.38 ± 0.59	1.45
12	109.113495	−9.413931	1.98 ± 0.33	5.15 ± 0.84	3.17 ± 2.30	0.006 ± 0.015	1.35 ± 4.10	5.45 ± 0.45	1.92
13	109.128975	−9.413376	2.28 ± 0.27	9.48 ± 1.19	8.09 ± 1.15	0.002 ± 0.005	0.16 ± 0.16	7.63 ± 0.46	8.45
14	109.131577	−9.409706	3.09 ± 0.33	11.14 ± 1.26	3.71 ± 1.64	0.013 ± 0.019	1.43 ± 1.42	6.33 ± 0.16	4.45
15	109.123474	−9.403764	4.64 ± 1.01	4.65 ± 0.27	0.17 ± 0.13	0.007 ± 0.017	3.88 ± 3.88	13.49 ± 0.39	17.58
16	109.114693	−9.401979	3.16 ± 0.63	11.39 ± 2.68	5.24 ± 1.99	0.002 ± 0.010	2.85 ± 3.59	4.85 ± 0.58	2.38
17	109.141520	−9.475020	0.60 ± 0.79	3.46 ± 0.59	0.10 ± 0.13	0.007 ± 0.008	28.69 ± 28.04	5.40 ± 0.27	8.85
18	109.166450	−9.448670	1.89 ± 0.53	6.59 ± 2.74	3.32 ± 3.21	0.036 ± 0.028	52.65 ± 39.97	4.95 ± 0.96	4.35
19	109.123810	−9.457560	2.57 ± 0.74	8.61 ± 3.76	4.66 ± 1.20	0.000 ± 0.000	0.06 ± 0.05	6.22 ± 1.13	1.95
20	109.123770	−9.449440	1.88 ± 0.46	5.20 ± 0.40	4.82 ± 2.52	0.007 ± 0.011	1.15 ± 1.05	4.34 ± 0.32	3.15
21	109.094720	−9.441330	4.79 ± 0.10	16.04 ± 0.21	4.07 ± 0.28	0.000 ± 0.000	0.00 ± 0.00	3.10 ± 0.34	11.15
22	109.111640	−9.437610	3.57 ± 0.38	12.30 ± 3.08	5.73 ± 2.30	0.000 ± 0.002	0.07 ± 0.07	6.75 ± 1.31	25.51
23	109.102440	−9.412630	3.60 ± 0.30	12.38 ± 3.06	5.91 ± 2.26	0.000 ± 0.000	0.03 ± 0.03	6.76 ± 1.32	6.45
24	109.088880	−9.398560	1.22 ± 0.54	4.18 ± 0.58	0.07 ± 0.28	0.038 ± 0.034	37.83 ± 37.80	6.20 ± 0.76	10.51
25	109.116930	−9.391600	3.62 ± 0.29	12.97 ± 1.09	4.29 ± 1.94	0.000 ± 0.000	0.00 ± 0.00	5.81 ± 0.84	8.67
T1	109.132507	−9.440776	2.27 ± 1.22	4.97 ± 0.59	3.10 ± 2.38	0.014 ± 0.015	7.91 ± 7.90	5.33 ± 0.62	13.29
T2	109.127251	−9.426885	2.32 ± 0.58	6.90 ± 1.91	4.37 ± 2.55	0.011 ± 0.017	34.07 ± 33.95	3.34 ± 0.71	2.63
T3	109.166985	−9.420988	5.87 ± 0.96	5.10 ± 0.65	0.16 ± 0.12	0.052 ± 0.086	149.58 ± 149.45	11.40 ± 1.01	6.23
T4	109.130173	−9.419502	1.82 ± 0.90	5.39 ± 2.27	0.80 ± 1.26	0.026 ± 0.028	73.84 ± 73.34	10.08 ± 0.83	8.87
T5	109.125168	−9.414126	0.76 ± 0.42	4.00 ± 0.43	0.29 ± 1.09	0.004 ± 0.009	4.28 ± 4.27	3.54 ± 0.35	7.74
C1	109.162000	−9.428901	8.78 ± 1.67	6.12 ± 1.61	0.04 ± 0.04	0.199 ± 0.274	390.00 ± 383.00	23.70 ± 6.69	35.89
C2	109.098038	−9.426320	2.81 ± 0.78	4.51 ± 0.19	0.17 ± 0.09	0.008 ± 0.018	6.94 ± 6.94	6.16 ± 1.35	10.15
C3	109.111923	−9.424769	2.66 ± 1.93	5.82 ± 4.75	0.37 ± 1.03	0.034 ± 0.048	112.23 ± 110.78	14.17 ± 1.21	18.19

predict that all three sources are young ($\lesssim 0.4 \times 10^5$ yr) and have relatively massive disks in comparison to the Class II sources of the region. The age estimation of the accreting embedded protostars is probably more uncertain and therefore should be considered as a quantitative indicator of stellar youth. Though we do not have sufficient data to address the evolutionary status of other Class I YSOs (C4, C5, and C6), the infrared colors of these objects indicate that they must be IR excess stars with a circumstellar disk. Here, we assume that the age of C4, C5, and C6 must be of the order of a few $\times$ 10^5 yr, which is generally attributed to this class of sources (Kenyon et al. 1990; Kenyon & Hartmann 1995). As discussed earlier, most of the Class I sources are distributed away from the central cluster. The Class I sources represent a much younger population than the ionizing source ($\sim 4 \times 10^6$ yr) and the associated Class II sources within the cluster region. It is also apparent from Table 2 that the disk accretion rate of the Class II YSOs, except for a few outliers, is in the range of 10^{-7} to 10^{-9} $M_\odot$ yr^{-1}, which is less than that of Class I/II and Class I YSOs (10^{-6} to 10^{-7} $M_\odot$ yr^{-1}). It is to be noted that in the absence of far-infrared (FIR) to millimeter data, the above values, particularly the disk parameters, should be treated with caution.

3.6. Massive YSOs

Samal et al. (2007), on the basis of MIR to FIR fluxes, predicted the presence of a massive zero-age main-sequence (ZAMS) star in region #1. In the *Spitzer* image, we identified a luminous source (C1; [3.6] = 12.1 mag) located behind the rim-like structure seen in the 5.8 μm image (see Figure 5). The star is faint in the K_s band and does not have a stellar counterpart in the optical. The SED models of the source based on data from 2MASS (J, H, and K_s), *Spitzer* (3.6, 4.5, and 5.8 μm), the *MSX* survey (14.65 and 21.30 μm), and AKARI (65, 90, 140, and 160 μm) are shown in Figure 6 (right panel). The SED of this YSO candidate is better sampled at longer wavelengths, showing a very steep rise in the 1.22 μm to $\sim$140 μm range, indicating the presence of an envelope; thus, the object should be a Class I YSO. The parameters from the best-fit models suggest that the source has an age of $\sim 4 \times 10^4$ yr and mass ~ 9 $M_\odot$ with a total luminosity of $\sim 1.8 \times 10^3$ $L_\odot$. The source is embedded in a cloud having $A_V \sim 24$ mag and is still accreting with a high envelope accretion rate of $\sim 9.8 \times 10^{-4}$ $M_\odot$ yr^{-1}. Accreting protostars show the signature of outflow in their very young age. Extended 4.5 μm emission often used as a tracer of outflow activity from massive young stellar objects (MYSOs), as the 4.5 μm IRAC band contains both H$_2$ ($v = 0$–0, $S(9,10,11)$) lines and CO ($v = 1$–0) band heads, thus can be excited by shocks such as those expected from protostellar outflows (Cyganowski et al. 2008, and references therein). Outflow sources identified based on their enhanced extended 4.5 μm emission are known as "Extended Green Objects (EGOs)" and are generally identified with color coding using IRAC three-color composite images. In search of EGOs, we made a color composite (see Figure 7)
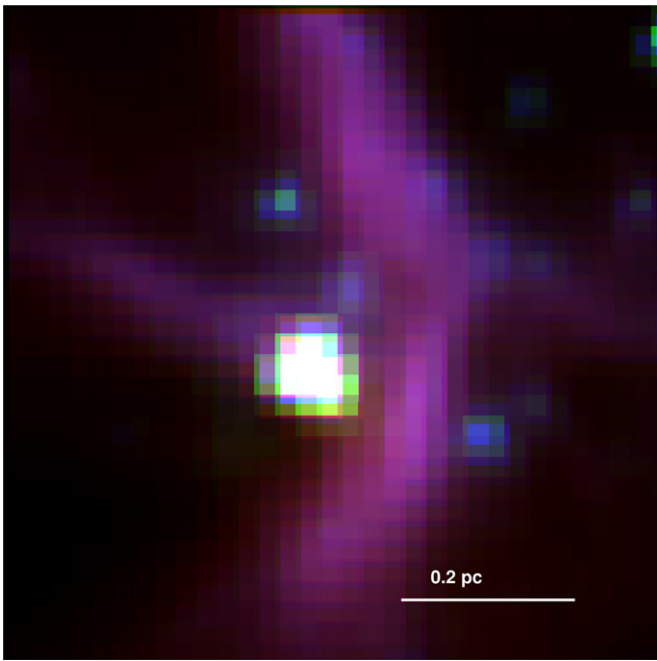
Figure 7. *Spitzer*-IRAC color composite image (5.8 μm, red; 4.5 μm, green; and 3.6 μm, blue) around the massive source C1. North is up and east is to the left.

(A color version of this figure is available in the online journal.)

image using the first three IRAC bands around the MYSO "C1." The source is embedded in a PDR, and PDRs are generally bright in IRAC 5.8 μm and 8.0 μm, thus adding to the difficulty of searching for weak EGOs. In Figure 7, however, we did not find any enhanced emission at 4.5 μm, indicating that the emission is either absent or very weak. It has been noted that the YSOs responsible for outflows appear blue in the IRAC [3.6]–[4.5]/[4.5]–[5.8] CC diagram and are generally located at a specific position ([3.6]–[4.5] $\geqslant$ 1.1 mag and [4.5]–[5.8] $\leqslant$ 0.8 mag; Ybarra & Lada 2009 and references therein) in this CC space and thus are sometimes used with caution to identify the driving sources. A comparison shows that none of the YSO candidates in our sample are located at the preferred position as mentioned above, in the IRAC [3.6]–[4.5]/[4.5]–[5.8] CC diagram (see Figure 2(b)), indicating that the identified YSOs have probably crossed the outflow stage. A star of $\sim$9 $M_\odot$ takes $\sim$2 $\times$ 10^5 yr to reach ZAMS (Bernasconi & Maeder 1996), and the evolutionary status (age < 10^5 yr) of the MYSO based on SED models indicates that the source is still in the PMS phase or about to reach ZAMS. In the PMS phase, the Lyman continuum emission from a massive star is expected to be much lower than its corresponding MS phase. In Paper I, we found a radio continuum peak in the proximity of structure #1; however, the emission is elongated along the bright arc seen in the 5.8 μm image. The *Spitzer* image reveals that massive source C1 does not exactly coincide with the radio peak, but is rather situated $\sim$20$''$ away in the eastern direction. Though the resolution of the radio continuum image presented in Paper I does not allow us to conclude about the origin of the radio emission, we presume that its elongated structure and its offset from source C1 possibly represent the ionized gas from the photoevaporating layer of the externally ionized rim (e.g., Morgan et al. 2004). The high envelope accretion rate indicates that source C1 may become more massive with time and may drive an H II region.

4. DISCUSSION ON STAR FORMATION ACTIVITY

Star formation in a molecular cloud is more active during the first few million years of a cloud's lifetime. It is believed that a majority of the stars in a molecular cloud form in clusters and, after a few million years of star formation, the gas in a molecular cloud dissipates and further star formation no longer takes place (Lada & Lada 2003). It is found that clusters with age greater than $\sim$5 $\times$ 10^6 yr are seldom associated with molecular gas (Leisawitz et al. 1989); thus, it is more likely that after $\sim$5 $\times$ 10^6 yr no gas is left over to form new stars. However, these types of molecular cloud complexes can still have star formation in PDRs at the interface of the H II region and the molecular gas. Many young clusters associated with H II regions show age spread, which is partly due to the cluster evolution and partly due to different epochs of star formation within the region (e.g., Sharma et al. 2007; Pandey et al. 2008; Jose et al. 2008). In the Sh2-294 region, with the help of *Spitzer* observations, we detected sources with a disk and envelope, evidence of youth of the region. The presence of extremely young Class I sources perhaps represents fresh star formation in the region. The SED models, within the uncertainties, indicate that the ages of most of the Class II YSOs are comparable to those of an ionizing source and that these sources are certainly older than Class I YSOs. All the Class I sources are distributed at the outskirts of the Sh2-294 region; most of them are associated with arc-shaped H$_2$ structures and PAH features. The distribution of young YSOs at the outskirts of H II regions/bubbles has been noticed in several cases (see, e.g., Deharveng et al. 2005, 2009; Zavagno et al. 2006; Koenig et al. 2008; Watson et al. 2008; Chauhan et al. 2011), where it is believed that the majority of them are formed as a result of triggered star formation. Although kinematics of the Sh2-294 region is not available, the morphology and the association of Class I YSOs with H$_2$ structures and their younger ages with respect to a 4 $\times$ 10^6 yr massive B0 MS star give evidence in favor of triggered star formation in the region. On the basis of *Hipparcos* data, Madsen et al. (2002) calculated the velocity dispersion of $\sim$1 km s^{-1} for stars in young clusters and associations. Since the Class I sources are expected to be young ($\sim$10^5 yr), their positions should roughly indicate the place where they were born, whereas with a velocity dispersion of 1 km s^{-1}, the Class II YSOs (median age $\sim$4.5 $\times$ 10^6 yr) might have drifted away $\sim$4 pc from their original position. Therefore, some of the Class II YSOs distributed away from the cluster center ($\alpha_{2000} = 07^h16^m33^s$, $\delta_{2000} = -09°25'35''$; see Samal et al. 2007) might have drifted due to their motion. Figure 5 shows the spatial distribution of YSOs. The Class I source C4 is associated with structure #2 and is situated at the vertex of a finger-like structure pointing toward the ionization source. A similar example can be seen in the case of RCW 120 (Zavagno et al. 2007; Deharveng et al. 2009), where a YSO is located at the vertex of a structure pointing toward the exciting star (Deharveng et al. 2009). Deharveng et al. (2009) proposed that the structure results from the dynamical instability of the expanding ionization front (IF), such as those simulated by Garcia-Segura & Franco (1996). Regions #1 and #3 are associated with Class I sources. Region #1 is associated with a relatively massive ($\sim$9 $M_\odot$) star and is more prominent in PAH emission than region #3, which is associated with a less massive ($\sim$2.7 $M_\odot$) star. The Class II source 25 seems to be projected near the H$_2$ structure #4, but its parameters derived from the acceptable SED-fitting models suggest that the source is possibly not embedded within the structure.

Though the spatial distribution and evolutionary status of YSOs argue in favor of triggered star formation, with the present data it is not possible to pinpoint the exact nature of triggering, but it is worth discussing the two most likely scenarios that might have happened in this region. In the first case, we discuss the star formation as seen in remnants of pre-existing molecular material of a parental clumpy cloud due to interaction of an expanding H II region. In the second case, we discuss the evolution of an H II region in a filament and the resulting star formation.

In the Sh2-294 region, we have identified structures (#1 and #3) with YSOs inside, and they resemble the numerical simulation of globules that resulted due to the impact of UV photons from the nearby massive OB stars on the pre-existing dense molecular material (Lefloch & Lazareff 1994). Structure #1 clearly shows an externally heated rim, with a massive $(9\,M_\odot)$ source C1 inside the rim, whereas region #3 has a more globular morphology, with a less massive $(2.7\,M_\odot)$ source C3 inside. In both cases, the structures show cometary morphology with their heads pointing toward the illuminating B0 MS star. Both structures are approximately at the same distance from the ionizing source. The different morphological structures under the same set of initial conditions and exposed to approximately the same amount of ionizing photons may be due to the differences in size and mass of the pre-existing clumps. Several studies show the association of YSOs with bright rims at the borders of H II regions (Sugitani & Ogura 1994; Ogura et al. 2002), and their formation is more likely due to the effect of strong external radiation from OB stars (Morgan et al. 2004; Urquhart et al. 2006). On the basis of cometary morphology, location, and age difference between the associated YSOs and the ionization source, one can anticipate that radiation-driven implosion (RDI; Lefloch & Lazareff 1994; Miao et al. 2006) could be the process of star formation for regions #1 and #3.

To evaluate this hypothesis, we quantitatively compare the time elapsed during the formation of the Class I YSO (C1) in region 1 with the age of the B0 ionization source at the center. In the case of RDI-induced star formation, the pre-existing molecular clumps are surrounded by high-pressure ionized gas due to the photoionizing UV photons, and the pressure exerted on the surface of the molecular clump leads to formation of a cometary globule. At an appropriate time, the high pressure will drive a shock front into the clump, leading to the formation of new stars (for details, see Lefloch & Lazareff 1994). We estimated the time needed for the IF to travel to the present position of the rim of structure #1 situated at a projected distance of 1.7 pc as $\sim 1.5 \times 10^5$ yr, assuming that the IF expands at the sound speed of 11.4 km s^{-1}. The characteristic timescale for producing cometary morphologies of various shapes and inducing gravitational collapse varies from 0.1 to $\sim 1 \times 10^6$ yr (Lefloch & Lazareff 1994; Miao et al. 2009), depending on initial conditions. Hence, we presume that the elapsed time to initiate star formation inside region #1 could be $\leqslant 1 \times 10^6$ yr. The age of the Class I source inside the rim should be of the order of 10^5 yr. Taken together, the summed timescale ($\sim 2.6 \times 10^6$ yr) is less than the age ($\sim 4.0 \times 10^6$ yr) of the ionizing source that powers the H II region. We also evaluated the shock crossing time to the globule to see whether the star formation in regions #1 and #3 started due to the propagation of the ionization-shock front or whether it had already taken place prior to the IF arrival. Assuming a typical shock velocity of 1–2 km s^{-1}, as found in the case of bright-rimmed clouds (see, e.g., Thompson et al. 2004; White et al. 1999) for the neutral gas associated with #1, the shock travel time to source C1 projected at a distance

~ 0.31 pc from the photoionization surface layer ranges from $(3.0$ to $1.5) \times 10^5$ yr. This timescale is comparable to the age of source C1. These simple approximate estimations suggest that the formation of source C1 and similarly C3 can be possible via the RDI mechanism.

Now we will discuss the bipolar H II region and its importance in star formation processes. In the bipolar case, it is most likely that the H II region forms in the dense region of a filamentary cloud, where the density along the equatorial axis of the filament is high, whereas it is low in the polar directions, leading to a high-density contrast. As a consequence, matter can be more compressed in the equatorial plane during the expansion of the H II region, depending on the initial density and ionization radiation from the H II region. A prototype example of such a bipolar morphological H II region is "Sh2-201," where two dense ($> 10^{22}$ cm^{-2}) and massive ($> 70\,M_\odot$) condensations are found on each side of the waist of Sh2-201 (Deharveng et al. 2012). Sh2-201 is believed to be formed in a large filament that is running east–west of Sh2-201. Massive condensations are the potential sites of new star formation. Indeed, Deharveng et al. (2012) detected two $100\,\mu$m point sources possibly of Class 0 nature in the east condensation ($\sim 235\,M_\odot$) and hypothesized that the triggered star formation is in fact at the waist of Sh2-201, which seems to be in accordance with numerical simulations of triggered star formation in a filamentary cloud due to dynamical compression of an expanding H II region (see Fukuda & Hanawa 2000). In the absence of long-wavelength observations, it is tempting to make a guess about the shape and structure of the original cloud in which Sh2-294 was formed. However, the morphology of Sh2-294 at $8\,\mu$m and $22\,\mu$m on a smaller scale suggests that it might be filamentary in nature. Presuming that Sh2-294 formed in a filamentary cloud, we compared the observed properties with the numerical simulations. The numerical simulations by Fukuda & Hanawa (2000), including a wide variety of physical conditions, suggest that for typical conditions the H II region takes more than five times the sound crossing time ($t_{\rm cross}$: see Equation (19) of Fukuda & Hanawa 2000) to form the first-generation cores (i.e., cores at the waist) in a filament. The first-generation cores can be followed by two second-generation cores depending on the initial conditions due to the change in self-gravity in the filament. The second-generation cores in a magnetized cloud are expected to be separated from the first-generation cores by the wavelength of most probable fragmentation, which is 13 times the length scale (H; see Equation (18) of Fukuda & Hanawa 2000). The $t_{\rm cross}$ and H in the simulations of Fukuda & Hanawa (2000) depend on the sound speed and the central density of the cold filamentary cloud. In Sh2-294, we presume that the H$_2$ structures #1 and #3, situated ~ 1.7 and 1.8 pc away from the ionizing source along the long axis seen in $8\,\mu$m, perhaps represent the externally heated part of the condensations that is at the waist of Sh2-294. Assuming an effective sound speed ~ 0.6 km s^{-1}, as found in the central region of filaments (e.g., Heitsch et al. 2009; the observed velocity dispersion), and the average density $\sim 10^5$–10^4 cm^{-3} of the protocluster-forming clumps (e.g., Mueller et al. 2002; Motte et al. 2008) as the density of cluster-forming filaments, we estimated the length scale and sound crossing time for Sh2-294 as ~ 0.04–0.14 pc and $\sim (7.6$–$25) \times 10^4$ yr, respectively. The presence of second-generation cores cannot be assessed with the present data, but what we see today is certainly the presence of two possible H$_2$ structures (#1 and #3), with Class I YSOs (C1 and C3) inside of these structures. Assuming that these Class I YSOs resulted from the cores that might have

formed due to the dynamical compression of the expanding H II region as simulated by Fukuda & Hanawa (2000), we calculated the approximate time that might have elapsed in the entire process. In the simulations of Fukuda & Hanawa (2000), the time required to produce dense cores depends on several factors. We considered those models which include magnetic field and treat the formation of an H II region on the filament axis or very close to it ($<5H$) as well as impinging the filament axis with a kinetic energy. These models predict that the time required to produce two first-generation cores ($\rho > \sqrt{10}\ \rho_0$) is less than or equal to 10 times the crossing timescale, which is $\leqslant 2.5 \times 10^6$ yr in the present case. The age of the Class I YSOs is of the order of $\sim 10^5$ yr. Assuming that the age ($\sim 4 \times 10^6$ yr) of the ionizing source represents the age of the H II region, it seems that Sh2-294 is old enough to produce two cores, which perhaps further collapses to form the Class I YSOs.

The above discussion with the present limited observations, suggests that both hypotheses can be justified as being responsible for triggered star formation in the Sh2-294 region. It is difficult to conclude with the present observations which one is superior over the other, though we prefer triggered star formation at the waist of Sh2-294 in a filamentary cloud, as the overall morphology of Sh2-294 on a smaller scale resembles a filamentary cloud. However, proof of this would require additional information such as the determination of exact stellar properties of YSOs with infrared spectroscopic observations, a search for a possible filamentary cloud with deep FIR observations, and kinematics with high-resolution line observations.

5. SUMMARY

In Paper I, we studied the Sh2-294 region and properties of the associated central cluster. With the help of low-resolution radio continuum observations at 1280 MHz, mid- and far-infrared emissions from *MSX* and HIRES maps, and optical–NIR point-source analyses, we tried to understand, for the first time, the star formation scenario in the Sh2-294 region. In the present paper, the high-resolution *Spitzer* images, along with the H_2 image with VLT, reveal the presence of several dusty structures and four prominent H_2 arc-like structures. In this paper, we focus on the identification of YSOs and tried to constrain their physical properties using color–color selections and SED-fitting models. In this study, we identified 25 Class II, 6 Class I, and 5 Class I/II sources on the basis of *Spitzer* colors and estimated their basic parameters, such as age, mass, disk accretion rate, and extinction, using SED-fitting models. These parameters provide additional insight into the evolutionary status of these YSOs, thus helping us to establish a spatial and temporal correlation among the YSOs and the ionizing source of Sh2-294. The Class I sources are found to be preferentially situated at the periphery of the H II region and are associated with H_2 arc-like structures. We have also shown that the population of Class I sources is indeed young in comparison to the Class II YSO population and the B0 MS star at the center of the nebula. The Class I source associated with structure "#1" is a massive ($\sim 9\ M_\odot$) and deeply embedded ($A_V \sim 24$ mag) protostar, accreting currently with an envelope accretion rate of $\sim 9.8 \times 10^{-4}\ M_\odot$ yr^{-1}. From the morphology, the spatial distribution of YSOs, and the timescale involved, we discussed triggered star formation in the region with two possible scenarios. The overall morphology of Sh2-294 and the timescale involved suggest that the dynamical compression of a filamentary cloud by the expanding H II region, following the simulations of Fukuda & Hanawa (2000), might be the cause for

new star formation in the region. However, further observations are needed to confirm this possibility.

REFERENCES

Allen, L. E., Burton, M. G., Ryder, S. D., Ashley, M. C. B., & Storey, J. W. V. 1999, MNRAS, 304, 98
Allen, L. E., Calvet, N., D'Alessio, P., et al. 2004, ApJS, 154, 363
Bernasconi, P. A., & Maeder, A. 1996, A&A, 307, 829
Bessell, M. S., & Brett, J. M. 1988, PASP, 100, 1134
Chauhan, N., Ogura, K., Pandey, A. K., Samal, M. R., & Bhatt, B. C. 2011, PASJ, 63, 795
Chauhan, N., Pandey, A. K., Ogura, K., et al. 2009, MNRAS, 396, 964
Chrysostomou, A., Brand, P. W. J. L., Burton, M. G., & Moorhouse, A. 1992, MNRAS, 256, 528
Churchwell, E., Povich, M. S., Allen, D., et al. 2006, ApJ, 649, 759
Cutri, R. M., Skrutskie, M. F., van Dyk, S., et al. 2003, VizieR Online Data Catalog, 2246, 0
Cyganowski, C. J., Whitney, B. A., Holden, E., et al. 2008, AJ, 136, 2391
Deharveng, L., Zavagno, A., Anderson, L. D., et al. 2012, A&A, submitted
Deharveng, L., Zavagno, A., & Caplan, J. 2005, A&A, 433, 565
Deharveng, L., Zavagno, A., Schuller, F., et al. 2009, A&A, 496, 177
Egan, M. P., Price, S. D., Kraemer, K. E., et al. 2003, VizieR Online Data Catalog, 5114, 0
Fazio, G. G., Ashby, M. L. N., Barmby, P., et al. 2004a, ApJS, 154, 39
Fazio, G. G., Hora, J. L., Allen, L. E., et al. 2004b, ApJS, 154, 10
Flaherty, K. M., Pipher, J. L., Megeath, S. T., et al. 2007, ApJ, 663, 1069
Fukuda, N., & Hanawa, T. 2000, ApJ, 533, 911
Garcia-Segura, G., & Franco, J. 1996, ApJ, 469, 171
Giard, M., Bernard, J. P., Lacombe, F., Normand, P., & Rouan, D. 1994, A&A, 291, 239
Hartmann, L., Megeath, S. T., Allen, L., et al. 2005, ApJ, 629, 881
Heitsch, F., Ballesteros-Paredes, J., & Hartmann, L. 2009, ApJ, 704, 1735
Hillenbrand, L. A., Bauermeister, A., & White, R. J. 2008, in ASP Conf. Ser. 384, 14th Cambridge Workshop on Cool Stars, Stellar Systems, and the Sun, ed. G. van Belle (San Francisco, CA: ASP), 200
Jose, J., Pandey, A. K., Ojha, D. K., et al. 2008, MNRAS, 384, 1675
Kenyon, S. J., & Hartmann, L. 1995, ApJS, 101, 117
Kenyon, S. J., Hartmann, L. W., Strom, K. M., & Strom, S. E. 1990, AJ, 99, 869
Koenig, X. P., Allen, L. E., Gutermuth, R. A., et al. 2008, ApJ, 688, 1142
Lada, C. J. 1987, in IAU Symp. 115, Star Forming Regions, ed. M. Peimbert & J. Jugaku (Dordrecht: Kluwer), 1
Lada, C. J., & Lada, E. A. 2003, ARA&A, 41, 57
Lada, C. J., & Wilking, B. 1984, ApJ, 287, 610
Lefloch, B., & Lazareff, B. 1994, A&A, 289, 559
Leisawitz, D., Bash, F., & Thaddeus, P. 1989, ApJS, 70, 731
Luhman, K. L., Engelbracht, C. W., & Luhman, M. L. 1998, ApJ, 499, 799
Madsen, S., Dravins, D., & Lindegren, L. 2002, A&A, 381, 446
Meyer, M., Calvet, N., & Hillenbrand, L. A. 1997, AJ, 114, 288
Miao, J., White, G. J., Nelson, R., Thompson, M., & Morgan, L. 2006, MNRAS, 369, 143
Miao, J., White, G. J., Thompson, M. A., & Nelson, R. P. 2009, ApJ, 692, 382

Moffat, A. F. J., Fitzgerald, M., & Jackson, P. D. 1979, A&ASS, 38, 197
Morgan, L. K., Thompson, M. A., Urquhart, J. S., White, G. J., & Miao, J. 2004, A&A, 426, 535
Motte, F., Bontemps, S., Schneider, N., Schilke, P., & Menten, K. M. 2008, in ASP Conf. Ser. 387, Massive Star Formation: Observations Confront Theory, ed. H. Beuther, H. Linz, & T. Henning (San Francisco, CA: ASP), 22
Mueller, K. E., Shirley, Y. L., Evans, N. J., II., & Jacobson, H. R. 2002, ApJS, 143, 469
Muench, A. A., Lada, C. J., Luhman, K. L., Muzerolle, J., & Young, E. 2007, AJ, 134, 411
Ogura, K., Sugitani, K., & Pickles, A. 2002, AJ, 123, 2597
Ojha, D. K., Samal, M. R., Pandey, A. K., et al. 2011, ApJ, 738, 156
Pandey, A. K., Sharma, S., Ogura, K., et al. 2008, MNRAS, 383, 1241
Robitaille, T. P. 2008, in ASP Conf. Ser. 387, Massive Star Formation: Observations Confront Theory, ed. H. Beuther, H. Linz, & T. Henning (San Francisco, CA: ASP), 290
Robitaille, T. P., Whitney, B. A., Indebetouw, R., & Wood, K. 2007, ApJS, 169, 328
Robitaille, T. P., Whitney, B. A., Indebetouw, R., Wood, K., & Denzmore, P. 2006, ApJS, 167, 256
Saito, H., Tamura, M., Kandori, R., et al. 2009, AJ, 137, 3149
Samal, M. R., Pandey, A. K., Ojha, D. K., et al. 2007, ApJ, 671, 555
Samal, M. R., Pandey, A. K., Ojha, D. K., et al. 2010, ApJ, 714, 1015
Sharma, S., Pandey, A. K., Ojha, D. K., et al. 2007, MNRAS, 380, 1141
Siess, L., Dufour, E., & Forestini, M. 2000, A&A, 358, 593
Sugitani, K., & Ogura, K. 1994, ApJS, 92, 163
Sugitani, K., Tamura, M., Nakajima, Y., et al. 2002, ApJ, 565, L25
Tej, A., Ojha, D. K., Ghosh, S. K., et al. 2006, A&A, 452, 203
Thompson, M. A., White, G. J., Morgan, L. K., et al. 2004, A&A, 414, 1017
Urquhart, J. S., Thompson, M. A., Morgan, L. K., & White, G. J. 2006, A&A, 450, 625
Walter, F. M., & Barry, D. C. 1991, in The Sun in Time, ed. C. P. Sonnett et al. (Tucson, AZ: Univ. Arizona Press), 633
Watson, C., Povich, M. S., Churchwell, E. B., et al. 2008, ApJ, 681, 1341
White, G. J., Nelson, R. P., Holland, W. S., et al. 1999, A&A, 342, 233
Whitney, B. A., Wood, K., Bjorkman, J. E., & Cohen, M. 2003a, ApJ, 598, 1079
Whitney, B. A., Wood, K., Bjorkman, J. E., & Wolff, M. J. 2003b, ApJ, 591, 1049
Wright, E. L., Eisenhardt, P. R. M., Mainzer, A. K., et al. 2010, AJ, 140, 1868
Yamamura, I., Makiuti, S., Ikeda, N., et al. 2009, in ASP Conf. Ser. 418, AKARI, a Light to Illuminate the Misty Universe, ed. T. Onaka et al. (San Francisco, CA: ASP), 3
Ybarra, J. E., & Lada, E. A. 2009, ApJ, 695, 120
Yun, J. L., Djupvik, A. A., Delgado, A. J., & Alfaro, E. J. 2008, A&A, 483, 209
Zavagno, A., Deharveng, L., Comerón, F., et al. 2006, A&A, 446, 171
Zavagno, A., Pomarès, M., Deharveng, L., et al. 2007, A&A, 472, 835